Under consideration for publication in *Electrophoresis...*

Effect of DC dielectrophoresis on the trajectory of a non-conducting colloidal sphere in a bent pore

Dustin L. House and Haoxiang Luo[1]

Department of Mechanical Engineering, Vanderbilt University
2301 Vanderbilt Pl, Nashville, TN 37235-1592, USA

Abstract

Dielectrophoresis has shown a wide range of applications in microfluidic devices. Force approximations utilizing the point-dipole method in dielectrophoresis have provided convenient predictions for particle motion by neglecting interactions between the particle and its surrounding electric and flow fields. The validity of this approach, however, is unclear when the particle size is comparable to the characteristic length of the channel and when the particle is in close proximity to the channel wall. To address this issue, we apply an accurate numerical approach based on the boundary-element method (BEM) to solve the coupled electric field, flow, and particle motion. This method can handle much closer particle–wall distances than the other numerical approaches such as the finite-element method. Using the BEM and integrating the Maxwell stress tensor, we simulate an electrokinetic, spherical particle moving within a bent cylindrical pore to investigate how the dielectrophoretic force affects the particle's trajectory. In the simulation, both the particle and the channel wall are non-conducting, and the electric double layers adjacent to the solid surfaces are assumed to be thin with respect to the particle radius and particle–wall gap. The results show that as the particle becomes close to the wall, its finite size has an increasingly important effect on its own transient motion and the point-dipole approximation may lead to significant error.

Keywords: dielectrophoresis, boundary-element method, Maxwell stress tensor, microfluidics

1 Introduction

Direct current (DC) based dielectrophoresis (DEP) is one of the popular methods to provide a manipulating force to accurately control the transport of biological particles in microchannels [1]. Despite the number of applications in microfluidic devices, modeling and characterization of dielectrophoresis for particle handling is still a challenging task. This is especially the case for arbitrary channel geometries and large particle-to-channel size ratios, which causes significant distortion of the local electrical and flow fields. Nevertheless, microfluidic channels often use complex geometries and small design features for the intricate manipulation of suspended particles. For example, Kang *et al.* [2] investigated the DEP effect of an insulating hurdle on the trajectory of electrophoretic polystyrene particles. Their objective was to use the DEP force generated near the corners of the hurdle to "push" the particles into different streamlines. The effect was introduced as a separation technique due to the fact that the streamline shift was dependent upon the size of the particle. To extend the study, the same group used a similar technique to separate white blood cells, and in a separate experiment, breast cancer cells [3]. A more adjustable form of DC-DEP was realized by Barbulovic-Nad *et al.* [4] by using an oil droplet as the insulating hurdle. In that study, adjusting the droplet size allowed for simple dynamic control of the field gradient used to generate

[1]Corresponding author. Email: haoxiang.luo@vanderbilt.edu Tel: +1-615-322-2079 Fax: +1-615-343-6687

the DEP force. Other non-trivial microfluidic networks utilize serpentine channels [5], spiraling channels [6] and converging–diverging sections [7] to attain the field distributions necessary for DEP particle manipulation in DC or DC-biased alternating fields.

Since resolving the particles in a numerical simulation is in general computationally demanding when modeling their transport in microchannels. For this reason, simplified approaches have been developed. For example, some researchers choose to take advantage of a similitude between the electric field and the fluid velocity field for electroosmotic flows [8–10]. By assuming that the particles in such flows simply follow the streamlines, the solution to the electric field alone may be used to approximate the particle motion [11, 12]. When the DEP effect on the particles is considered, a further approximation is to employ the the point dipole or multipole methods [13] to determine the DEP force. In these methods, the particle size is assumed to be infinitely small, and the DEP force can be evaluated based on a simple formula involving the undisturbed local electric field strength and its derivatives. Under these approximations, the particle's trajectory can be found by performing straightforward Lagrangian tracking. To improve the accuracy of this approach, sometimes an empirical correction factor is used to correct the particle mobility [14, 15]. The point-particle approach can be highly efficient and is valid when the size of the particle is small when compared to that of the channel. However, as the particle is close to the wall, or its size approaches that of the channel, distortion of the surrounding electric field due to the presence of the particle can no longer be neglected. For example, when a non-conducting particle is close to a plane wall, it has been shown in experiments that a net DEP force is generated from the distorted electric field in the narrow gap between the particle and wall [16]. This force is in addition to the DEP generated by the global nonuniformity of the electrical field. Some previous studies have shown that the dipolar or multipole approximation of the DEP leads to inaccuracies when applied to a particle in the vicinity of an electrode [17, 18]. Similar to the DEP approximation, ignoring the particle's presence in the flow field may oversimplify the hydrodynamics and lead to inaccurate estimate of the viscous drag on the particle. For these reasons, a study addressing the DEP mobility of particles of finite size would have to fully couple the particle together with the electric field and flow. So far there are only a few limited such studies [7, 19].

For electrokinetic particles of finite sizes, both analytical and computational approaches have been applied previously to solve the governing equations and to obtain description of the particle dynamics. For example, exact solutions [20, 21] and asymptotic expansions [22–24] have been applied to obtain expressions of the velocity or force on a spherical particle near a planar or cylindrical geometry. For an arbitrary geometrical configuration, a numerical technique is necessary to simulate the flow and electric field. Numerical methods based on volume discretization such as the finite-element method (FEM) have limited accuracy when the particle–wall separation is small compared to the particle size and a fine resolution is needed to resolve the gap region. Additionally, for transient simulations, the volume mesh often has to be regenerated every few time steps to avoid severe mesh distortion. On the other hand, the boundary–element method (BEM) [25], which requires a surface mesh only, is superior to the FEM in accuracy and efficiency when a linear problem is considered, e.g., an electrokinetic problem with the assumption of thin electric double layers (EDL). Previously, the BEM has been adopted in the study of electrokinetic flows [26–28] and has shown useful applications. We also have developed an in-house BEM code to solve electrokinetics of particles in arbitrary channels [29]. The numerical approach can handle very small gap region (around 1% of the particle size). With slight modification, the solver can incorporate the Maxwell stress tensor and can thus be used to simulate the DEP effect on the

particle.

The purpose of this work is to study the fundamental effect of DC-DEP on particle motion in microchannels where the electric field is non-uniform due to both local channel geometry and presence of the particle. A non-conducting spherical particle driven by electrophoresis in a bent cylindrical pore is chosen as the basic configuration for this study. The BEM solver is used to solve the electrokinetic flow and integrate the Maxwell stress tensor. Governing parameters, including the size and initial position of the particle and the electric field strength, will be systematically varied to investigate the DEP effect. In a closely related study, Ai *et al.* [19] investigated the DEP effect on the transient dynamics of an electrophoretic particle in an L-shaped rectangular channel. Using two-dimensional (2D) simulations, they also studied the effects of the particle size, initial location, and electric field strength. Compared to their work, the present study solves a three-dimensional (3D) flow rather than using a 2D approximation. A 3D study is motivated by several important differences in both the surrounding Stokes flow and the electric field when comparing an infinite cylinder and a sphere. For example, when there is a bounding wall nearby, the fluid within the gap between the particle and wall experiences much less viscous impedance for a sphere than for a cylinder due to the 3D effect. However, the electric field in the gap is much stronger for the cylinder. The opposing effects thus complicate the problem at hand. In fact, Keh *et al.* [30] showed that the electrophoretic mobility of a non-conducting near-wall cylindrical particle is much higher than that of a sphere, especially when the particle–wall gap is small. In their work, the translational velocity of the cylinder is 37% higher than that of the sphere when $a/d = 0.9$ (a is radius of the particle and d is the distance from the particle's center to the wall), and the difference between the rotational velocity is even higher (about a factor of 4 when $a/d = 0.9$). Our own calculation using the BEM method shows that the DEP force on a cylinder increases much faster than the DEP on a sphere as they are closer to a plane wall (at $a/d = 0.5$, the normalized DEP force is 0.07 for 3D but is 0.46 for 2D, and at $a/d = 0.98$, the force is 2.12 for 3D but is 23.49 for 2D). In the current study, the small particle–wall gap, whose minimum is on order of 1% of the particle radius, is well resolved using the highly accurate boundary-element method, while in Ai *et al.* [19], the minimum gap appears to be more than 30% of the particle radius. This capability allows us to explore the smaller-gap situation where the DEP effect is much stronger. Finally, another important goal of the present work is to perform a comparison of the full numerical simulation with predictions based on the point-dipole method in an effort to provide a clear view of the limitations associated with the latter method.

2 Problem specification and governing equations

We consider a spherical particle suspended in an aqueous electrolyte solution within a cylindrical channel, as shown in Figure 1(a). The problem configuration is three-dimensional where the particle is free to rotate and translate in the plane of symmetry. Both the particle and the channel wall are non-conducting and carry uniform surface charges, which are characterized by their respective zeta potentials, ζ_p and ζ_w. A positively charged surface has a positive value of zeta potential. We assume that the thickness of the EDL, i.e., the Debye length k^{-1}, adjacent to the particle surface and wall is much smaller compared to the particle size and to the particle–wall gap width so that there is no EDL overlapping and the thin-EDL approximation may be used. With this approximation, the entire flow field is neutral, and the distribution of the electric potential, ϕ, is governed by the Laplace equation $\nabla^2\phi = 0$. The electric potential is subject to the homogeneous

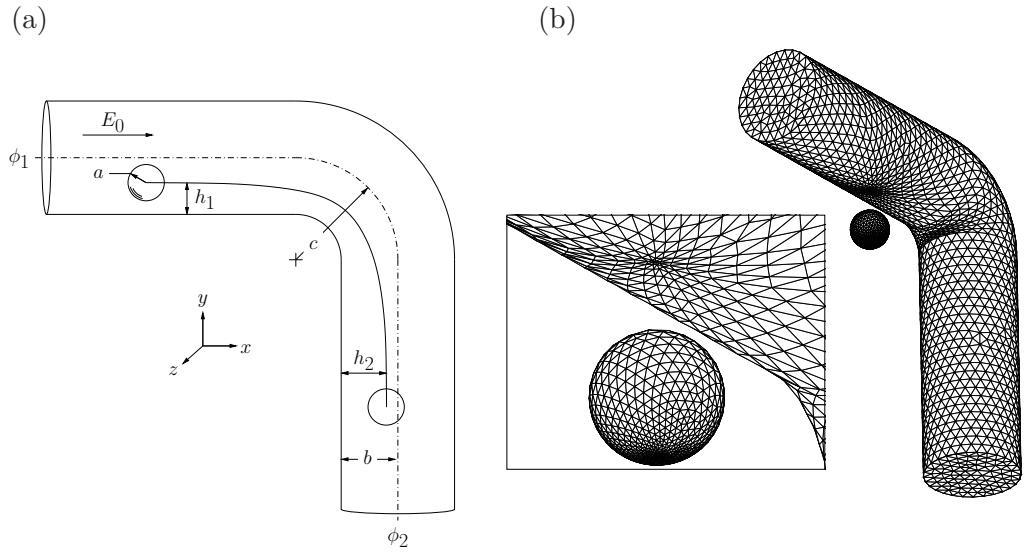

Figure 1: (a) Schematic of a non-conducting particle moving through a cylindrical pore. (b) The adaptive mesh (note that the particle is translated outside for better visualization).

Neumann boundary condition, $\partial\phi/\partial\mathbf{n} = 0$, at the particle surface and channel wall [23], and a constant potential is specified at the inlet, $\phi = \phi_1$, and also at the outlet, $\phi = \phi_2$. Note that $\mathbf{n}$ is the surface normal and points into the flow.

The fluid is assumed to be Newtonian and incompressible, and the Reynolds number is small so that the fluid inertia can be ignored. The bulk flow is then governed by the Stokes and continuity equations, $-\nabla p + \mu\nabla^2\mathbf{u} = 0$ and $\nabla \cdot \mathbf{u} = 0$, where p, $\mathbf{u} = (u_x, u_y, u_z)$, and μ are the pressure, velocity, and viscosity, respectively. Under the thin-EDL assumption, the fluid velocity next to the particle or channel wall can be expressed as a slip velocity that is relative to the solid surface and is proportional to the local tangential gradient of the electric potential [31], $\mathbf{u}^S = \frac{\varepsilon\zeta}{\mu}(\mathbf{I}-\mathbf{nn})\cdot\nabla\phi$, where $\mathbf{u}^S$ is the slip velocity, ε is the dielectric constant of the electrolyte solution, $\zeta = \zeta_p$ or ζ_w is the zeta potential on either the particle surface or channel wall, and $(\mathbf{I}-\mathbf{nn})$ is the surface gradient operator. In the laboratory coordinates, the fluid velocity at the particle surface is the combination of the rigid-body motion of the particle and the slip velocity, $\mathbf{u}(\mathbf{x}) = \mathbf{u}^B + \mathbf{u}^S = \mathbf{u}_c + \omega\mathbf{e}_z \times (\mathbf{x} - \mathbf{x}_c) + \mathbf{u}^S$, in which $\mathbf{x}$ is a point on the particle surface, $\mathbf{x}_c$ and $\mathbf{u}_c$ are the position and velocity of the centroid of the particle, ω is the rotational speed of the particle, $\mathbf{e}_z$ is the unit vector in z, and $\mathbf{u}^B = \mathbf{u}_c + \omega\mathbf{e}_z \times (\mathbf{x} - \mathbf{x}_c)$ is the velocity of the point $\mathbf{x}$ due to the rigid body motion. The particle is assumed to be neutrally buoyant in the fluid and has negligible inertia. Thus, the total traction and torque on the particle vanish. The local traction includes both the hydrodynamic traction and the Maxwell stress tensor [32], $\mathbf{T} = \varepsilon(\mathbf{EE} - \frac{1}{2}|\mathbf{E}|^2\mathbf{I})$, with ε being the dielectric constant of the electrolyte solution and $\mathbf{I}$ the unit tensor.

3 Boundary integral formulation and numerical approach

The equations governing the electric potential and the Stokes flow are solved using a boundary-element approach [25, 33]. The integral formulation is presented in our earlier publication [29]. To discretize the integral equations, the particle surface, cylinder wall, and the inlet and outlet

are represented using six-node curved triangular elements [33]. The unknown variables pertinent to the electric field, i.e., ϕ at the particle and wall surfaces and $\partial\phi/\partial\mathbf{n}$ at the inlet/outlet, are discretized at the six vertices of the elements. The unknown variables pertinent to the flow, i.e., the hydrodynamic traction, are discretized at the element centroids. At each time step, the integral equation for the electric potential is solved first. Then, the slip velocity at all surfaces and the Maxwell stress are found by computing the gradient of ϕ numerically. In the end, the flow is solved together with unknown translational and rotational velocities of the particle. To match the total number of unknowns, two additional equations expressing the total traction and the total torque on the particle are appended to the linear algebraic system. Integrals over each element are carried out using the Gauss–Legendre quadratures, and the resulting linear equation systems are solved using the LAPACK library. Once the solutions on the particle and pore surfaces are obtained, the potential and fluid velocity at any interior point of the flow, if needed, can be calculated in a post-processing process. The temporal update of the velocity and position of the particle is achieved using a second-order Runge–Kutta scheme. The element size of the mesh used in this study is adaptive and is based on the particle's proximity to the wall. That is, the local resolution of the mesh around the particle–wall gap, including both the particle and wall surfaces, is increased to make sure that the small region is resolved sufficiently (see Figure 1(b)). Finally, it should be pointed out the current boundary-element solver is based on a free online library, BEMLIB [33].

4 Results and Discussions

4.1 Code validation

In order to validate the accuracy of the present BEM code, we compared our results with those published previously. Three problems for which an analytical solution is available were chosen for the test.

In first two tests, we consider the configuration of a non-conducting spherical particle suspended in an electrolyte and positioned near an infinite non-conducting plane wall. Solutions for these tests are compared in Table 1. In the first test, we calculate the "wall-enhanced" electrophoretic velocity U_p reported by Keh and Chen [20] for the particle when translating steadily along the plane wall (by deactivating the Maxwell stress in the code). In the second test, the lateral dielectrophoretic force F_{dep} of the particle is calculated and compared with that reported by Young and Li [21]. Both of these effects have to do with the distortion of the electric potential in the narrow gap between the particle and wall. For these tests, the code was slightly modified to calculate the disturbance potential and flow field caused by introducing the particle. This technique is described in more detail in a previous report [29].

For the first test, the normalized translational mobility is tabulated in Table 1(a) as a function of a/d, where a is the particle radius and d is the distance from the particle center to the wall. From this comparison, we can see the mobility decreases to a minimum before increasing to values greater than that of an unbounded particle. This is consistent with the analytical solution represented by the eigenfunction expansion series in the bipolar coordinates [20]. It should be noted that the closest particle–wall separation simulated in the current study was $a/d = 0.99$. Even in this case, the difference between our numerical solution and the analytical solution is only less than 0.2%.

The second comparison, tabulated in Table 1(b), is the normalized DEP force acting in the lateral direction as a function of a/d. Here we can see that the lateral force monotonically increases with a decreasing gap width. This trend agrees with the exact solution originally obtained by

(a)

	$U_p\mu/[\varepsilon(\zeta_p-\zeta_w)E_0]$	
a/d	Current study	Keh & Chen [20]
0.50	0.994	0.994
0.70	0.988	0.989
0.90	0.997	0.998
0.95	1.022	1.022
0.98	1.080	1.080
0.99	1.147	1.145

(b)

	$F_{dep}/[\varepsilon E_0^2 a^2/2]$	
a/d	Current study	Young & Li [21]
0.50	0.074	0.075
0.71	0.336	0.337
0.91	1.133	1.136
0.95	1.584	1.587
0.98	2.121	2.124
0.99	2.457	2.459

Table 1: Comparison with the analytical solutions for an electrophoretic particle near a plane wall.

Young and Li [21]. Similar to the electrophoretic validation, superb accuracy was achieved. For the closest particle–wall separation simulated in the current study, $a/d = 0.99$, the difference between our result and the analytical result is less than 0.1%.

The domain used in the present study consists of a spherical particle within a cylindrical pore, so it is also appropriate to conduct a validation for such an enclosed geometry. Thus, our third test concerns a non-conducting spherical particle of radius a driven by electrophoresis within a straight cylinder of radius b. Our numerical result was compared with the analytical result reported by Keh and Chiou [34], who found the fundamental solution and then applied the Fourier transform and a collocation method to solve the problem. The cylinder in our test was truncated so that its length is six times its own diameter. The comparison is shown in Table 2, where it can be seen that the non-dimensional electrophoretic mobility of the particle monotonically decreases as the radius of the particle increases. This pore-impedance effect parallels that discussed by Keh and Chiou and is caused by the hydrodynamic retardation due to the presence of the wall. Again, the numerical results are in excellent agreement with the analytical solution.

	$U_p\mu/[\varepsilon(\zeta_p-\zeta_w)E_0]$	
a/b	Current study	Keh & Chiou [34]
0.1	1.000	0.999
0.2	0.990	0.990
0.3	0.966	0.969
0.4	0.928	0.932
0.5	0.872	0.880

Table 2: Electrophoretic mobility of a sphere concentrically positioned within a cylindrical pore.

4.2 Simulation setup

For the current study, the cylindrical pore has a radius b, and the turning radius, c, as measured from the cylinder's centerline, is $c/b = 1.2$. The total length of the cylinder along the centerline is $L/b = 12$, and the bend takes place in the middle of the cylinder. The nominal electric field strength, $E_0 = (\phi_1 - \phi_2)/L$, is used as a variable of study. The non-dimensional form adopted for

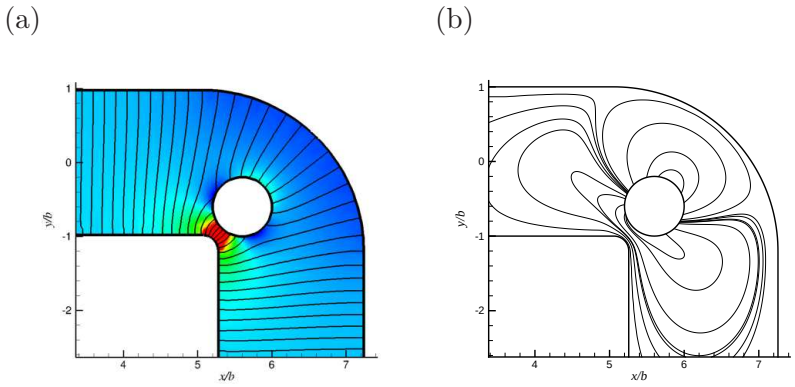

Figure 2: (a) Equipotential contours plotted over the electric field strength and (b) flow streamlines around a particle ($a/b = 0.4$ and $\zeta_w = 0$) positioned close to the inner wall.

this variable is $E_0^* = E_0 b/(\zeta_p - \zeta_w)$. In the simulations, 1294 elements were used on the particle and 4026 elements on the cylinder wall. Sufficiency of the described mesh in resolving small particle–wall gap distances has been demonstrated in the validation tests. After extensive testing, a time step of $\Delta t = 0.05a/U_p$, where $U_p = \varepsilon(\zeta_p - \zeta_w)E_0/\mu$, was utilized for transient simulations to ensure Δt was small enough to accurately predict the particle's trajectory. To illustrate the results obtained from the BEM code, Figure 2 shows the electric potential and flow field computed after the boundary-element solution was obtained for an arbitrarily specified particle location. It can be seen that the electric field is distorted due to presence of the particle.

To justify the need for the full numerical simulation, we also compare our particle trajectory with that predicted by the point-dipole method (PDM). When using the PDM, the DEP force is calculated as if the particle were not present and both the electric field and the flow field were undisturbed. The motion of the particle, which is approximated by an infinitesimal point, is then a combination of the Smoluchowski velocity (electrophoretic translation of an unbounded particle), $\mathbf{u}_{ep}$, the electroosmotic velocity, $\mathbf{u}_{eof}$, and the velocity due to the DEP force, $\mathbf{u}_{dep}$,

$$\mathbf{u} = \mathbf{u}_{ep} - \mathbf{u}_{eof} + \mathbf{u}_{dep} = \frac{\varepsilon\zeta_p}{\mu}\mathbf{E} - \frac{\varepsilon\zeta_w}{\mu}\mathbf{E} + \frac{\varepsilon a^2 f_{cm}}{3\mu}\nabla|\mathbf{E}|^2, \tag{1}$$

where f_{cm}, the Clausius–Mossotti function, is $-\frac{1}{2}$ for a non-conducting spherical particle [13]. In this formula, $\mathbf{u}_{dep}$ has been found by equating the DEP force with the Stokes drag assumed for the particle, that is,

$$\mathbf{F}_{dep} = 2\pi\varepsilon a^3 f_{cm}\nabla|\mathbf{E}|^2 = 6\pi\mu a\mathbf{u}_{dep}. \tag{2}$$

To evaluate Eq. (1), the field strength $\mathbf{E}$ of the undisturbed electric field at the location of the centroid of the particle is used for each term.

Note that in the current BEM simulation, neither the point-dipole approximation of the DEP force nor the Stokes drag is assumed for the finite-size particle. To show the difference between our numerical result and the point-dipole method, we use both methods for the instantaneous particle location in Figure 2 under a non-dimensional electric field of $E_0^* = 20$. The BEM method shows that $u_{ep}/U_p = 1.12$ and $u_{dep}/U_p = 0.48$, while the approximations in Eq.(1) claim $u_{ep}/U_p = 1.25$ and $u_{dep}/U_p = 1.51$. Therefore, ignoring the particle's size may lead to significant error in the DEP mobility.

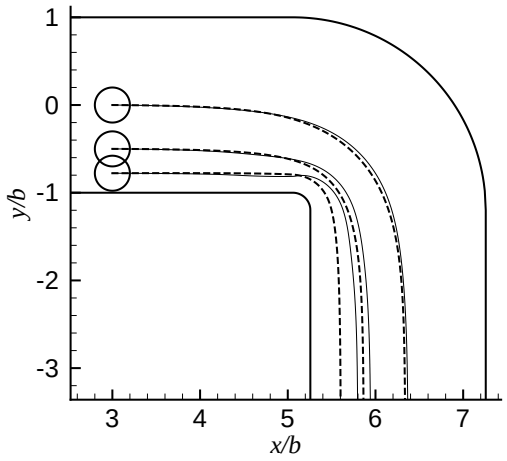

Figure 3: The effect of the initial position, h_1/b, on the particle trajectory for $a/b = 0.2$ and $E_0^* = 5$. Dashed lines represent results found using the BEM, and the solid lines represent the prediction by the PDM.

4.3 Effect of the initial location

The first parameter studied was the eccentricity of the particle. In this section we wanted to observe the effect that the particle's initial location had on its trajectory. We are also interested in the ability of the point-dipole method to predict this effect. For these simulations, the particle's radius was held constant at $a/b = 0.2$ while the initial location of the particle was adjusted to three different values: $h_1/b = 1.0$, 0.5 and 0.22. Note that in the third case, the initial particle–wall gap is 10% of the particle radius. The results of these tests are presented as dashed lines in Figure 3 for the case of $E_0^* = 5$.

While approaching the exit of the pore, the final deviation of each particle from its original location was found to be $(h_2 - h_1)/h_1 = 0.08$, 0.22, and 0.56, respectively for the three cases. As anticipated, a particle positioned closer to the inner side of the bent region will deviate farther from the wall than a particle originally positioned closer to the center of the pore. Similar to Figure 2, the highest electric field strength here is found in the region within the cylinder close to the inside of the bend. It follows that the dielectrophoretic force acting on a particle closer to that region would be greater because this force scales with $|\mathbf{E}|^2$. The particle originally positioned with the highest eccentricity is shifted by a distance equal to 62% of its own radius. Considering the scenario of a stream of multiple particles, each with a different initial location, this effect would serve to reduce the width of the particle stream in a focusing effect by pushing the near-wall particles away from the wall.

The analogous trajectories found using the PDM are displayed as solid lines in Figure 3. It is clear from this figure that the PDM fails to accurately predict the path of the particle positioned close to the cylinder wall. When observing each trajectory with respect to the particle's original position, we can see that the accuracy of this method degrades with a decreasing particle–wall gap. The final deviations as shown in the figure are $(h_2 - h_1)/h_1 = 0.11$, 0.37 and 1.44 for $h_1/b = 1.0$, 0.5 and 0.22, respectively. Although the PDM overshoots the particle's deviation in each of the

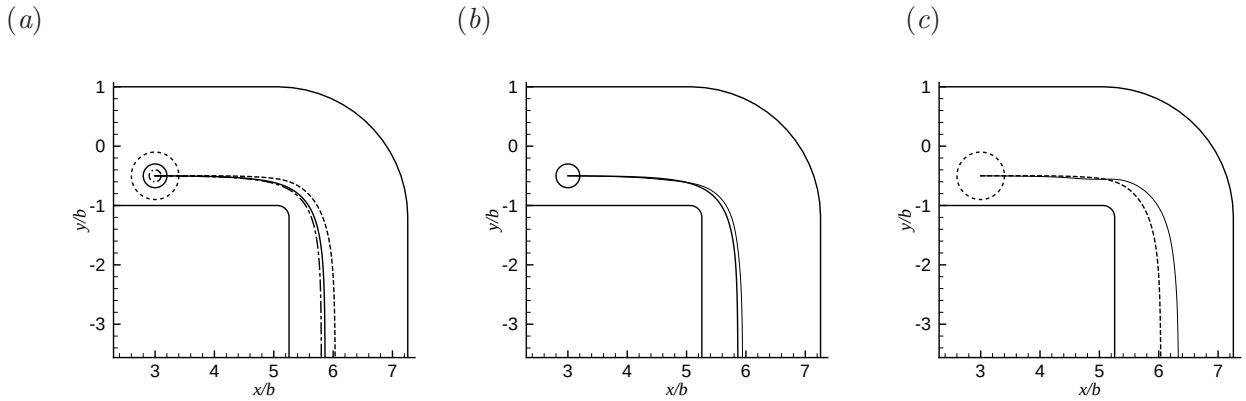

Figure 4: The effect of the particle size, a/b, on the particle trajectory for the case of $h_1/b = 0.5$ and $E_0^* = 5$. Dash-dotted, solid (thick), and dashed lines represent $a/b = 0.1$, 0.2, and 0.4 respectively in (a). In (b-c) the thin-solid line represents the estimate from the PDM.

cases tested, it does provide a reasonable approximation for the case of the particle positioned at the center of the pore.

4.4 Effect of particle size

In scaling, the dielectrophoretic force is also proportional to the volume of the insulating particle. Therefore it is also of interest to study how the particle's radius affects its trajectory. In the present study, this effect is complicated by the manner in which the particle's insulating volume modifies the flow and electrical field. Three particle-to-cylinder radius ratios were tested in this section: $a/b = 0.1$, 0.2 and 0.4. The same original position was used for each of the particles, $h_1/b = 0.5$, and the nominal electric field was held constant at $E_0^* = 5$. The resulting trajectory for each case can be seen in Figure 4(a). As one would expect, the larger particle shifts toward the centerline of the pore to a greater extent when compared to the smaller particles. The final deviations from the wall are $(h_2 - h_1)/h_1 = 0.09$, 0.22 and 0.56 for the three cases respectively. Note that this result is similar to the 2D simulation by Ai *et al.* [19] for a cylindrical particle in a rectangular channel.

We also calculated the trajectory of the particle based on the PDM to evaluate its validity. Figures 4(b) and (c) show a comparison between the trajectories found using the BEM and the PDM for each particle size. The thin-solid line shows the PDM result, whereas the line patterns for the BEM result follow those of Figure 4(a). From Figures 4(b), it is apparent that at sufficiently small particle sizes, the PDM can provide a reasonable approximation of its trajectory in this configuration. For $a/b = 0.1$, the difference in the trajectories predicted by the two methods is less than 1% of the pore radius. For $a/b = 0.2$, this difference is roughly 8%. Observing Figure 4(c), however, we can conclude that utilizing the PDM leads to significant error for the case of a large particle. The final difference between the two techniques for the case of $a/b = 0.4$ is approximately 30% of the pore radius.

To more clearly visualize the difference in the results of the two methods, Figure 5 plots the magnitude of the normalized DEP force as a function of the non-dimensional time as the particle migrates through the dashed trajectory shown in Figure 4(c). Both the BEM calculation (dashed line) and the point-dipole estimate (solid line) of the DEP force are plotted. It can be seen from

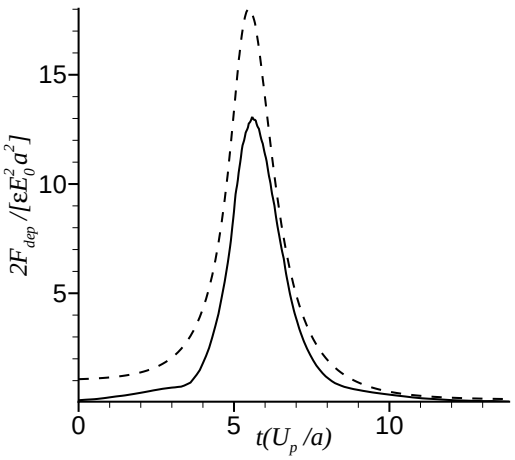

Figure 5: The normalized DEP force as the particle moves along the trajectory shown in Figure 4(c) from the BEM simulation (dashed line) and the point-dipole estimate (solid line).

Figure 5 that during the initial stage, the BEM yields a DEP force whereas the PDM does not. At this phase, the particle is positioned close to the inside of the wall just before the bend. The presence of the particle causes a strong electric field in the narrow region, which generates a DEP force acting laterally and pushes the particle away from the wall. This result is similar to the flat-wall case described earlier in Table 1(b). When using the PDM, there is no such particle–wall interaction and therefore there is no DEP force.

As the particle nears the inside corner of the bend, the magnitude of the DEP force quickly increases to a maximum before decreasing as it leaves the turn. This occurs because of the non-uniform electric field originating from the insulating boundary. During this phase, the current technique reports a stronger DEP force compared to the PDM. Again, the enhanced DEP can be explained by the interaction between the finite-size particle and the wall.

It is important to note that although the resultant DEP force is stronger when using the Maxwell stress tensor compared to the PDM, the former does not result in greater lateral motion of the particle compared to that found from the PDM. On the contrary, the trajectory predicted by the PDM overshoots as shown in Figure 5 and thus indicates a higher lateral velocity. This result can be explained by the use of the Stokes drag in Eq. (2) to equate with the DEP force in the PDM. Because the spherical particle in this study is bounded by the pore of comparable sizes and is near a wall, the actual hydrodynamic drag acting on the particle will be greater than that predicted by Stokes drag.

In Figure 5, after the particle passes through the turn, the DEP forces given by both the BEM and PDM decrease to approximately zero. This is because the particle is positioned near the center and there is little particle–wall interaction. Thus, the two methods agree with each other.

4.5 Effect of the electric field

In the present problem, the local electrical field strength is linearly proportional to the global field strength. Thus, raising E_0 will cause the DEP force on the particle to increase quadratically. To

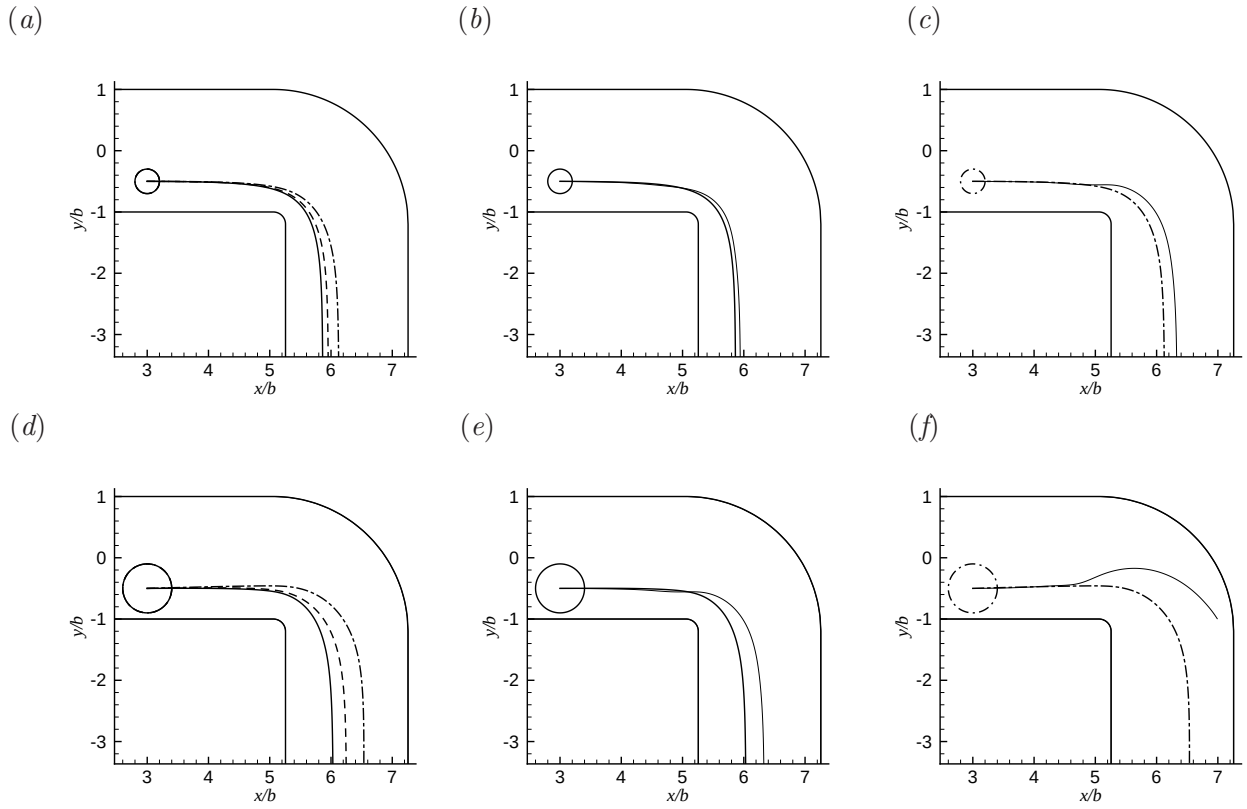

Figure 6: Trajectories for $a/b = 0.2$ (a-c) and $a/b = 0.4$ (d-f) under varying electric field strengths but the same initial position, $h_1/b = 0.5$. (a) and (d) depict the cases of $E_0^* = 5$, 10, and 20 using solid, dashed, and dot-dashed lines respectively. A comparison between the PDM and BEM is shown for the cases of $E_0^* = 5$ (b,e) and 20 (c,f), where the thin-solid line represents the PDM trajectory and the line patterns of the BEM trajectories follow those introduced in (a) and (d).

	$a/b = 0.2$		$a/b = 0.4$	
E_0^*	Current study	PDM	Current study	PDM
5	1.35	1.38	1.41	1.53
10	1.38	1.44	1.50	1.68
20	1.45	1.53	1.61	—

Table 3: Deviation of trajectory, $(h_2 - h_1)/h_1$, for both the point-dipole method and the BEM used in this study for the cases in Figure 6.

study the effect of E_0 on the particle's trajectory, we use two different particle sizes, $a/b = 0.2$ and 0.4, and vary E_0^* between 5 and 20. The results are shown in Figure 6. With an increasing electric field strength, we can expect that the particle will deviate farther from the inner wall of the pore. This is verified in Figure 6(a) and (d) for the cases of $a/b = 0.2$ and 0.4 respectively. The applied electric field values shown in both Figure 6(a) and (d) correspond to $E_0^* = 5$, 10, and 20 with line patterns of thick-solid, dashed, and dash-dotted, respectively. For these results the particle's initial location within the pore is $h_1/b = 0.5$. From Figure 6(a), we can see that the stronger the electric field is, the more the particle would translate laterally across the pore. From Figure 6(d) we can see the combined effect of the electric field strength on the larger particle, $a/b = 0.4$. Similar to the case of $a/b = 0.2$, the particle also deviates from the inner wall to a greater extent with an increasing field strength. However, the deviation for $a/b = 0.4$ is much higher than that for $a/b = 0.2$. Note that this result is qualitatively in agreement with the 2D simulation by Ai *et al.* [19] for a cylindrical particle in a rectangular channel.

In the numerical method implemented in this study, the local distortion of the electric field due to the presence of the non-conducting particle is accounted for by integrating the Maxwell stress tensor around the particle surface. As the point-dipole approach neglects this distortion, we would expect that the disagreement between the two methods would grow with an increasing electric field strength. Figures 6(b) and (c) depict the comparison for $E_0^* = 5$ and 20 and $a/b = 0.2$. Continuing in the comparison of the particle size, Figures 6(e) and (f) show the results of equivalent simulations at $a/b = 0.4$. Again, the thin-solid line visualizes the PDM result and the line patterns for the BEM result follow those of Figures 6(a) and (d). Under a weaker electric field, the magnitude of the dielectrophoretic force is reduced and therefore the field distortion is not as influential. Therefore, the PDM and BEM give a similar result, as shown in Figure 6(b). However, it is evident from Figure 6(c) that under the influence of a stronger electric field of $E_0^* = 20$, the difference between the two methods is greater than 20% of the pore radius and thus the accuracy of the PDM has degraded.

As the particle-to-cylinder ratio and the electric field strength are both increased, the difference between the PDM prediction and the BEM simulation becomes substantially large, which is shown by Figures 6(e) and (f). Table 3 provides a quantitative comparison of the BEM and PDM results in terms of the deviation defined as $(h_2 - h_1)/h_1$ for the cases in shown Figure 6. Note the deviation for $E_0^* = 20$ and $a/b = 0.4$ is not available for the PDM because it finally breaks down, as seen in Figure 6(f) where the particle tends to cross the wall. In a physical situation, as a finite-size particle approaches the outer wall, the DEP effect on the inner-wall side would decrease and on the other hand, the opposing DEP due to the outer wall would increase. As a result, the overall

DEP force in the lateral direction becomes zero, and the particle would not come into contact with the outer wall. As shown in Figure 6(f), this effect is captured by the current BEM simulation but not by the point-dipole approximation. In summary, the combined effect of E_0 and a/d in such a simple but non-trivial microfluidic channel demands full integration of the Maxwell stress tensor in order to predict the particle dynamics accurately.

5 Conclusion

To investigate the fundamental effect of dielectrophoresis on the transient motion of particles in microfluidic channels and to address limitation of the point-dipole approximation in the particle simulation, we have considered a non-conducting spherical particle in a 90° bent cylindrical pore, where the size of particle is comparable to the pore diameter. The electric double layer is assumed to be thin, and its effect is approximated by a slip velocity on the particle and pore surfaces.

To accurately account for the finite size of the particle and handle small particle–wall gaps, we have applied a highly accurate boundary-element method to solve the Stokes flow as well as the electric field, and the dielectrophoretic force is obtained by integrating the Maxwell stress tensor over the particle surface. The simulation results show that near the corner of the wall, the DEP force has a strong effect on the particle's motion. More importantly, for near-wall situations the particle's finite size has a significant effect on its transient trajectory, and using the point-dipole approximation would lead to substantial error.

As a final discussion, we would like point out the relevance of our model to real microchannels. For a commonly used aqueous, symmetric electrolyte solution (e.g. KCl) with an ionic concentration of 10^{-3} M and its chemical and electrical properties [35, 36] at room temperature, the EDL thickness (k^{-1}) would be on the order of 10 nm. If we consider a 20 μm diameter particle, this would yield $ka \approx 1000$, well within the limits of the thin-EDL approximation. In the present study, the minimum gap width occurring between the particle and the channel wall is around 2% of the particle radius, that is, approximately 0.2 μm, which still roughly 20 times the thickness of the EDL. If we extend this dimensional discussion to include other parameters used in the present study for the case of $a/b = 0.2$, then the diameter and length of the pore are $2b = 100$ μm and $L = 600$ μm. Assuming common electrical properties of polystyrene for the particles ($\zeta_p = -22$ mV), PDMS for the channel walls ($\zeta_w = -80$ mV) and pure water for the suspending medium ($\epsilon = 6.9\times10^{-10}$ C/Vm, $\mu = 0.9 \times 10^{-3}$ kg/ms), the nominal electrical field strengths to generate the deviations described in this study are between $E_0 = 60$ and 240 V/cm. These values fall within a range of field strengths commonly used for DC-DEP. Under these operating conditions, one can expect to see electrokinetic particle velocities between 0.2 and 1 mm/s.

Acknowledgements

The present solver is heavily based on the BEMLIB, a free online software library developed by Professor C. Pozrikidis of University of Massachusetts, Amherst, whose effort is gratefully acknowledged. We would also like to thank Dr. Paulo Ferreira de Sousa for his assistance in the coding work.

References

[1] Srivastava S. K., Gencoglu A., Minerick A. R., *Anal. Bioanal. Chem.* 2011.

[2] Kang K. H., Xuan X., Kang Y., Li D., *J. Appl. Phys.* 2006, *99*, 064702.

[3] Kang Y., Li D., Kalams S. A., Eid J. E., *Biomed. Microdevices* 2008, *10*, 243–249.

[4] Barbulovic-Nad I., Xuan X., Lee J. S. H., Li D., *Lab Chip* 2006, *6*, 274–279.

[5] Church C., Zhu J., Wang G., Tzeng T. R. J., Xuan X., *Biomicrofluidics* 2009, *3*, 044109.

[6] Zhu J., Xuan X., *J. Colloid Interf. Sci.* 2009, *340*, 285–290.

[7] Ai Y., Qian S., Sheng L, Joo S. W., *Biomicrofluidics* 2005, *4*, 013201.

[8] Cummings E. B., Griffiths S. K., Nilson R. H., Paul P. H., *Anal. Chem.* 2000, *72*, 2526–2532.

[9] Santiago J. G., *Anal. Chem.* 2001, *73*, 2353–2365.

[10] Santiago J. G., *J. Colloid Interf. Sci.* 2007, *310*, 675–677.

[11] Cummings E. B., Singh A. K., *Anal. Chem.* 2003, *75*, 4724–4731.

[12] Kwon J. S., Maeng J. S., Chun M. S., Song S., *Microfluid. Nanofluid.* 2008, *5*, 23–31.

[13] Jones T. B., *Electromechanics of particles*, Cambridge University Press, Cambridge, UK 1995.

[14] Church C., Zhu J., Nieto J., Keten G., Ibarra E., Xuan X., *J. Micromech. Microeng.* 2010, *20*, 1–6.

[15] Çetin B., Li D., *Electrophoresis* 2010, *31*, 3035–3043.

[16] Lo Y. J., Lei U., *Appl. Phys. Lett.* 2010, *97*, 093702.

[17] Rosales C., Lim K. M., *Electrophoresis* 2005, *26*, 2057–2065.

[18] Al-Jarro A., Paul J., Thomas D. W. P., Crowe J., Sawyer N., Rose F. R. A., Shakesheff K. M., *J. Phys. D: Appl. Phys.* 2007, *40*, 71–77.

[19] Ai Y., Park S., Zhu J., Xuan X., Beskok A., Qian S., *Langmuir* 2010, *26*, 2937–2944.

[20] Keh H. J., Chen S. B., *J. Fluid Mech.* 1988, *194*, 377–390.

[21] Young E. W. K., Li D., *Langmuir* 2005, *21*, 12037–12046.

[22] Yariv E., Brenner H., *SIAM J. Appl. Math* 2003, *64*, 423–441.

[23] Yariv E., Brenner H., *J. Fluid Mech.* 2003, *484*, 85–111.

[24] Yariv E., *Phys. Fluids* 2006, *18*, 031702.

[25] Pozrikidis C., *Boundary integral and singularity methods for linearized viscous flow*, Cambridge University Press, New York 1992.

[26] Sellier A., *C. R. Acad. Sci. Srie IIb* 2001, *329*, 565–570.

[27] Allison S. A., Xin Y., *J. Colloid Interface Sci.* 2005, *288*, 616–628.

[28] Wong X., Rosales C., *Eng. Anal. Bound. Elem.* 2008, *32*, 388–394.

[29] House D. L., Luo H., *Eng. Anal. Boundary Elem.* 2010, *34*, 471–476.

[30] Keh H. J., Horng K. D., Kuo J., *J. Fluid Mech.* 1991, *231*, 211–228.

[31] Keh H. J., Anderson J. L., *J. Fluid Mech.* 1985, *153*, 417–439.

[32] Wang X., Wang X. B., Gascoyne P. R. C., *J. Electrostat.* 1997, *39*, 277–295.

[33] Pozrikidis C., *A practical guide to boundary element methods with the software library BEMLIB*, CRC Press, London, UK 2002.

[34] Keh H. J., Chiou J.Y., *AIChE. J.* 1996, *42*, 1397–1406.

[35] Ye C., Li D., *J. Colloid Interface Sci.* 2002, *251*, 331–338.

[36] Li D., *Electrokinetics in Microfluidics*, Elsevier, Burlington, MA 2004.